The Astrophysical Journal, 934:155 (10pp), 2022 August 1 https://doi.org/10.3847/1538-4357/ac7be3
© 2022. The Author(s). Published by the American Astronomical Society.
OPEN ACCESS

# Solar Magneto-seismology of a Magnetic Slab in an Asymmetric Magnetic Environment

Noémi Kinga Zsámberger[1,2,3] and Róbert Erdélyi[1,4,5]
[1] Solar Physics and Space Plasma Research Centre, School of Mathematics and Statistics, University of Sheffield, Hicks Building, Hounsfield Road, Sheffield, S3 7RH, UK; robertus@sheffield.ac.uk
[2] Department of Physics, University of Debrecen, 1. Egyetem tér, H-4010, Debrecen, Hungary
[3] Doctoral School of Physics, University of Debrecen, Egyetem tér 1., Debrecen, H-4010, Hungary
[4] Department of Astronomy, Eötvös Loránd University, 1/A Pázmány Péter sétány, H-1117 Budapest, Hungary
[5] Gyula Bay Zoltán Solar Observatory (GSO), Hungarian Solar Physics Foundation (HSPF), Petőfi tér 3., Gyula, H-5700, Hungary
*Received 2022 March 2; revised 2022 May 27; accepted 2022 June 2; published 2022 August 3*

## Abstract

Diagnosing the solar atmospheric plasma remains one of the major challenges in solar physics. In recent years, new methods have been developed to apply the powerful concept of solar magneto-seismology (SMS) to obtain information about plasma parameters in solar structures guiding magnetohydrodynamic (MHD) waves that would otherwise be difficult to measure. This paper uses the Cartesian model of a magnetic slab placed in an asymmetric magnetic environment to generalize recently discovered SMS techniques. Utilizing the fact that the asymmetric environment changes the character of the classical kink and sausage eigenmodes, we describe two spatial seismology methods built upon this mixed character of quasi-sausage and quasi-kink modes. First, we present the amplitude ratio technique, which compares the oscillation amplitudes measured at the two boundaries of the slab, and we provide expressions to estimate the internal Alfvén speed in the thin slab and in the incompressible plasma approximations. The second main technique relies on the changed distribution of wave power throughout the slab under the effect of waveguide asymmetry. This minimum perturbation shift technique is then also utilized to provide Alfvén speed estimates that depend on the plasma and magnetic parameters of the environment, as well as the measured slab width and oscillation frequency. Finally, we perform a brief investigation of how the amplitude ratio and the minimum perturbation shift depend on the different sources of waveguide asymmetry, and illustrate our findings with numerical results.

*Unified Astronomy Thesaurus concepts:* Solar physics (1476); The Sun (1693); Magnetohydrodynamics (1964); Solar atmosphere (1477); Solar coronal seismology (1994); Solar coronal waves (1995)

*Supporting material:* animations

## 1. Introduction

The atmosphere of our Sun is a complex plasma environment finely structured by its ubiquitous magnetic fields. In understanding and measuring the properties of this rich variety of solar waveguides, the constantly evolving methods of solar magneto-seismology provide a useful and versatile toolkit. These methods combine theoretical descriptions of magnetohydrodynamic (MHD) waves with data from their observational detections, and thus—through solving often difficult inversion problems—allow us to draw conclusions about "missing" parameters of the solar atmospheric plasma that would be otherwise difficult to obtain (see also Erdélyi 2006a, 2006b; Banerjee et al. 2007; Arregui & Goossens 2019).

Beyond their newer, diagnostic role, MHD waves have always been thought to play an important part in solving the puzzle of solar atmospheric heating as well. Reflecting this significance, the theory of MHD wave propagation developed rapidly (De Moortel & Nakariakov 2012), and soon these theories led to the early solar magneto-seismology (SMS) studies of the solar atmosphere (such as Rosenberg 1970; Roberts et al. 1984). Several of these investigations employed methods of temporal seismology, which encompasses various methods that rely on the observed frequency (or period) of MHD waves to be used in calculations of background quantities. An additional quantity that is of special importance to temporal seismology is the damping time of solar atmospheric oscillations. For example, similarly to Hollweg et al. (1990), Goossens et al. (2002) and Ruderman & Roberts (2002) investigated growth and damping times of kink waves due to resonant absorption and found that large-scale density inhomogeneities can cause oscillating loops to decay very swiftly and prevent them from showing pronounced oscillations.

The maximum available resolution limited the range of fine-scale results achievable by both temporal and spatial seismology. As one of the first examples of using performing solar atmospheric seismology based on spatial information, Uchida (1970) gave an estimate of the magnetic field structure in the solar corona based on observations and theoretical analyses of Moreton waves. More recent spatial techniques rely on detecting the wave power distribution of eigenfunctions corresponding to a theoretical model. A popular quantity to be utilized is the anti-node shift of standing modes in a magnetic flux tube, which makes it possible to diagnose the inhomogeneous density stratification of the tube (Erdélyi & Verth 2007; Verth et al. 2007; Erdélyi et al. 2014).

The field of SMS gained new impetus with the first imaging detection of transversal waves in coronal loops using the space-based TRACE [Transition Region and Coronal Explorer] observatory in 1998. The detected oscillations were classified as kink modes, although identifying them as fast magnetoacoustic waves was debated (Aschwanden et al. 1999; Nakariakov et al. 1999;

Original content from this work may be used under the terms of the Creative Commons Attribution 4.0 licence. Any further distribution of this work must maintain attribution to the author(s) and the title of the work, journal citation and DOI.

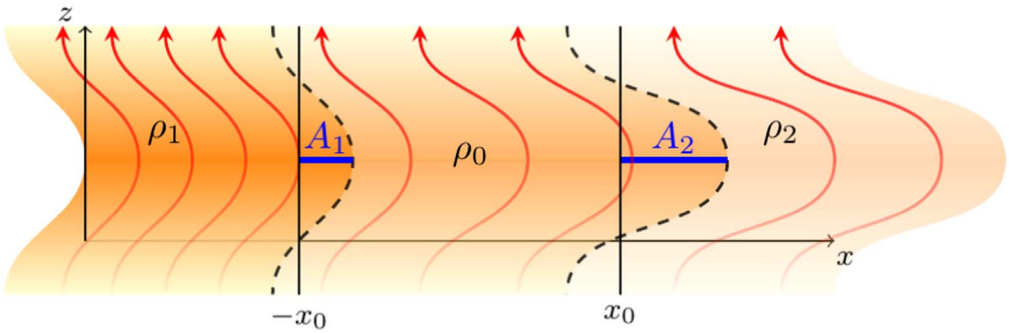


**Figure 1.** Illustration of the principle of the amplitude ratio method: the ratio of transverse displacement (or velocity) amplitudes at the two boundaries of the slab, $A_1$ and $A_2$, is calculated and measured.

Goossens et al. 2009). The recent golden age of SMS since TRACE has been characterized by steady improvements in both temporal and spatial resolution, as well as in the variety and availability of both space-based observatories, e.g., SOHO [Solar and Heliospheric Observatory], SDO [Solar Dynamics Observatory], and STEREO [Solar-TErrestrial RElations Observatory], as well as ground-based telescopes, e.g., DST [Richard B. Dunn Solar Telescope] and SST [Swedish Solar Telescope] (detailed further in comprehensive reviews such as Nakariakov & Verwichte 2005; Banerjee et al. 2007; Ruderman & Erdélyi 2009; Wang 2011; Arregui et al. 2012; De Moortel & Nakariakov 2012; Mathioudakis et al. 2013). The constantly improving observational capabilities have led to discovering wave-like perturbations in a plethora of solar atmospheric features, from large-scale structures like coronal loops or plumes to more localized phenomena such as spicules or regions within sunspots (Aschwanden 2005; Banerjee et al. 2007; Zaqarashvili, T. V., & Erdélyi, R 2009; Arregui 2015).

The two fundamental types of analytical models of solar magnetic structures used in SMS investigations are cylindrical flux tubes and Cartesian slabs. The construction and basics of slab models are summarized in a series of seminal articles written by Edwin & Roberts (1982) about an interface (Roberts 1981a) and a magnetic slab in a field-free environment (Roberts 1981b). This was further developed by Edwin & Roberts (1982), when they placed the slab in a magnetic environment. While all of these classical studies used symmetric environmental regions, their results were generalized by Allcock & Erdélyi (2017) when they introduced asymmetry into the nonmagnetic environment of a magnetic slab. Wave propagation in a slab in an asymmetric magnetic environment, as a new addition, was described by Zsámberger et al. (2018) and Zsámberger & Erdélyi (2020, 2021). Oxley et al. (2020a) and Oxley et al. (2020b) then investigated standing waves in asymmetric nonmagnetic and magnetic environments of magnetic slabs, respectively.

In the current paper, we provide a reminder of and further develop the SMS methods described in Allcock & Erdélyi (2018), applying them to the problem of wave propagation in an asymmetric magnetic slab. In Section 2, we focus on the distributions of the transverse velocity amplitudes of eigenmodes across the slab and provide an analytical description of the amplitude ratios of quasi-sausage and quasi-kink modes in the general case, as well as various limits of slab width and plasma-$\beta$ values. We also compare these approximations with results obtained from numerical solutions of the general dispersion relation. In Section 3, the same examination is then extended to the techniques based on the shifting of the minimally perturbed layer within the slab.

## 2. Amplitude Ratios

By generalizing the amplitude ratio method described in Allcock & Erdélyi (2018), this section aims to derive an expression describing the ratio of the transverse displacement or velocity amplitudes on the two boundaries of an asymmetric magnetic slab. In the following, we show how this ratio depends on the parameters of an observed oscillation in the slab waveguide, as well as on the physical and geometric attributes of the waveguide itself. The expression for the amplitude ratio is then utilized to estimate background parameters of the system. Figure 1 demonstrates the principle of the amplitude ratio method for a quasi-kink mode of a perturbed asymmetric magnetic slab waveguide.

The process through which we derive the amplitude ratio is formally similar to the method described in Allcock & Erdélyi (2018) and Allcock et al. (2019); however, due to the existence of asymmetric external magnetic fields in the model approximation studied here, both density and magnetic asymmetry are incorporated into the quantities we define (such as $m_j$, $\Lambda_j$, for $j = 0, 1, 2$, for their definition see below), which will become clear in the final result.

Zsámberger et al. (2018) as well as Zsámberger & Erdélyi (2020, 2021) investigated propagating waves in a magnetic slab enclosed in an asymmetric magnetic environment. This three-dimensional slab system is filled with inviscid, static, ideal plasma and permeated by equilibrium magnetic fields with a nonzero component only in the $z$-direction (along the slab). The equilibrium state of this slab model is described by

$$N(x) = \begin{cases} N_1 & x < -x_0, \\ N_0 & |x| < x_0, \\ N_2 & x_0 < x, \end{cases} \tag{1}$$

where $N_j$ stands for any of the following physical parameters: densities, $\rho$, pressures, $p$, temperatures, $T$, and magnetic field strengths, $\mathcal{B}$, within a given region of the slab. Furthermore, $N_j =$ constant (for $j = 0, 1, 2$), where quantities describing the inside of the slab are denoted by the subscript $j = 0$, while the parameters of the left- and right-hand-side regions carry the subscripts $j = 1,2$, respectively.

During the derivation of the dispersion relation detailed in Zsámberger et al. (2018), it was shown that the $x$-component of the velocity perturbation of trapped magnetoacoustic modes propagating along the slab has the form of $v_{j,x}(x, t) = \hat{v}_x(x)e^{i(kz-\omega t)}$, where $\hat{v}_x(x)$ is the transverse velocity amplitude given by a combination of the hyperbolic functions in each region of the slab

system, namely as

$$\hat{v}_x(x) = \begin{cases} A(\cosh m_1 x + \sinh m_1 x), & x < -x_0, \\ B\cosh m_0 x + C\sinh m_0 x, & |x| < x_0, \\ D(\cosh m_2 x - \sinh m_2 x), & x_0 < x, \end{cases} \tag{2}$$

with $A$, $B$, $C$, and $D$ being arbitrary constants. These constants can be determined (within one degree of freedom) by satisfying the four boundary conditions imposing the continuity of total pressure and velocity perturbations at the two interfaces separating the slab from its asymmetric environment. From the application of these boundary conditions, Zsámberger et al. (2018) obtained a system of four coupled, linear, homogeneous algebraic equations, which can be summarized as

$$\begin{bmatrix} C_1 - S_1 & -C_0 & S_0 & 0 \\ 0 & C_0 & S_0 & S_2 - C_2 \\ -\Lambda_1(C_1 - S_1) & -\Lambda_0 S_0 & \Lambda_0 C_0 & 0 \\ 0 & \Lambda_0 S_0 & \Lambda_0 C_0 & -\Lambda_2(S_2 - C_2) \end{bmatrix} \begin{bmatrix} A \\ B \\ C \\ D \end{bmatrix} = \begin{bmatrix} 0 \\ 0 \\ 0 \\ 0 \end{bmatrix}.$$

Here,

$$\begin{aligned} C_j &= \cosh(m_j x_j), \\ S_j &= \sinh(m_j x_j), \quad \text{and} \\ \Lambda_j &= -\frac{i\rho_j}{\omega}\frac{k^2 v_{Aj}^2 - \omega^2}{m_j} \qquad (\text{for } j = 0, 1, 2). \end{aligned} \tag{3}$$

From this, Zsámberger et al. (2018) obtained the dispersion relation for the asymmetric magnetic slab system by ensuring that the determinant of this matrix was zero. Satisfying the dispersion relation then allows one degree of freedom to be gained in the system of equations derived from the boundary conditions. This means that we may choose one of the constants, $B$ or $C$, as arbitrary. Depending on this choice, we will deal with either the quasi-sausage or the quasi-kink eigenmodes of the system, as detailed in Allcock & Erdélyi (2018) and briefly explained in the following sections.

### 2.1. Quasi-sausage Modes

For quasi-sausage modes, we let the constant $C$ be arbitrary, which allows us to determine the other three coefficients as

$$A = \frac{1}{C_1 - S_1}(BC_0 - CS_0), \tag{4}$$

$$D = \frac{1}{C_2 - S_2}(BC_0 + CS_0), \tag{5}$$

$$B = \frac{\Lambda_0 C_0 + \Lambda_1 S_0}{\Lambda_0 S_0 + \Lambda_1 C_0} C = -\frac{\Lambda_0 C_0 + \Lambda_2 S_0}{\Lambda_0 S_0 + \Lambda_2 C_0} C. \tag{6}$$

The second expression for $B$ in Equation (6) can be found by using the first expression in the same equation and the dispersion relation, which we restate here for ease of understanding:

$$2(\Lambda_0^2 + \Lambda_1\Lambda_2) + \Lambda_0(\Lambda_1 + \Lambda_2)\left[\tau_0 + \frac{1}{\tau_0}\right] = 0, \tag{7}$$

where

$$\tau_0 = \tanh(m_0 x_0). \tag{8}$$

If we substitute the first expression in Equation (6) into Equation (2) describing the transverse velocity amplitudes and take the values at the two interfaces, we obtain

$$\hat{v}_x(-x_0) = BC_0 - CS_0 = \frac{\Lambda_0}{\Lambda_0 + \Lambda_1(1/\tau_0)}\frac{1}{S_0}C, \quad \text{and} \tag{9}$$

$$\hat{v}_x(x_0) = BC_0 + CS_0 = \frac{\Lambda_0(\tau_0 + 1/\tau_0) + 2\Lambda_1}{\Lambda_0 + \Lambda_1(1/\tau_0)} C_0 C. \tag{10}$$

Similarly, we can freely choose to substitute the second expression from Equation (6) instead, and then the result is

$$\begin{aligned} \hat{v}_x(-x_0) &= BC_0 - CS_0 \\ &= -\frac{\Lambda_0(\tau_0 + 1/\tau_0) + 2\Lambda_2}{\Lambda_0 + \Lambda_2(1/\tau_0)} C_0 C, \quad \text{and} \end{aligned} \tag{11}$$

$$\hat{v}_x(x_0) = BC_0 + CS_0 = -\frac{\Lambda_0}{\Lambda_0 + \Lambda_2(1/\tau_0)}\frac{1}{S_0}C. \tag{12}$$

The two forms of the velocity perturbation amplitudes at the slab boundaries are equivalent. They express the magnitude as well as the direction of the transverse velocity perturbation, therefore they can be considered a signed amplitude, with positive values expressing perturbations in the positive $x$-direction, and vice versa.

For the ease of comparing the two configurations, we adopt the following definition of the amplitude ratio from Allcock & Erdélyi (2018):

$$R_A := \frac{\hat{\xi}_x(x_0)}{\hat{\xi}_x(-x_0)}, \tag{13}$$

which compares the displacement perturbation amplitude (defined as $\hat{\xi}_x(x) = i\hat{v}_x(x)/\omega$) at the right-hand-side interface to the amplitude at the left-hand-side interface. An equivalent definition can be given using the velocity perturbation amplitudes as

$$R_A := \frac{\hat{v}_x(x_0)}{\hat{v}_x(-x_0)}. \tag{14}$$

We substitute the simpler expressions for the velocity amplitudes at the boundaries, in which the denominators contain properties of the slab and one of the environmental regions (namely, $\Lambda_0$ and $\Lambda_1$, or $\Lambda_0$ and $\Lambda_2$, respectively), but the numerators only depend on the properties of the slab interior ($\Lambda_0$). Therefore, in the case of quasi-sausage modes, we substitute Equations (9) and (12) into the definition of the amplitude ratio (Equation (14)), which yields

$$R_A = -\frac{\Lambda_0 + \Lambda_1\frac{1}{\tau_0}}{\Lambda_0 + \Lambda_2\frac{1}{\tau_0}}, \tag{15}$$

or equivalently

$$R_A = -\frac{\rho_1 m_2}{\rho_2 m_1}\frac{\left[\frac{\rho_0}{\rho_1}m_1(k^2 v_{A0}^2 - \omega^2) + m_0(k^2 v_{A1}^2 - \omega^2)\frac{1}{\tau_0}\right]}{\left[\frac{\rho_0}{\rho_2}m_2(k^2 v_{A0}^2 - \omega^2) + m_0(k^2 v_{A2}^2 - \omega^2)\frac{1}{\tau_0}\right]}. \tag{16}$$

The amplitude ratio is negative, as in quasi-sausage modes, the displacement perturbations at the two boundaries of the slab happen in opposite directions. If the configuration is symmetric (and so the characteristic speeds and densities on the two sides are equal), this ratio reduces to $R_A = -1$, as expected, meaning that in the sausage modes of the symmetric slab system, the two boundaries oscillate exactly in anti-phase.

#### 2.1.1. Quasi-sausage Amplitude Ratio in the Thin-slab Approximation

Since the amplitude ratio is a measurable quantity, our main aim is to use it to determine a background parameter of the asymmetric waveguide we derived it for. This background parameter should be one that is not easy to observe directly, such as a magnetic field strength or Alfvén speed in the system. In order to provide an analytical approximation for one of these, we must restrict ourselves to various limiting cases of either slab width or plasma-$\beta$ parameters.

In the thin-slab limit, the wavelength of the oscillations is much longer than the width of the slab, that is, $kx_0 \ll 1$, and therefore $m_0 x_0 \ll 1$. Then, the coth function can be approximated by the reciprocal of its argument in Equation (16), so the amplitude ratio can be approximated as

$$R_A = -\frac{\rho_1 m_2}{\rho_2 m_1} \frac{\left[\frac{\rho_0}{\rho_1} m_1 x_0 (k^2 v_{A0}^2 - \omega^2) + (k^2 v_{A1}^2 - \omega^2)\right]}{\left[\frac{\rho_0}{\rho_2} m_2 x_0 (k^2 v_{A0}^2 - \omega^2) + (k^2 v_{A2}^2 - \omega^2)\right]}. \tag{17}$$

This makes it possible for us to express the internal Alfvén speed in the slab as a function of the external characteristic speeds and the densities, as well as the amplitude ratios, wavenumbers, and angular frequencies:

$$v_{A0}^2 = \frac{\omega^2}{k^2}\left[1 - \frac{\rho_1 m_2 (k^2 v_{A1}^2 - \omega^2) + R_A \rho_2 m_1 (k^2 v_{A2}^2 - \omega^2)}{\omega^2 x_0 m_1 m_2 \rho_0 (1 + R_A)}\right]. \tag{18}$$

Most quantities on the right-hand side are known or can be expressed as a function of other measurable quantities themselves. The right-hand side, in the end, depends on two wave parameters (wavenumber and angular frequency), the background temperatures, and the Alfvén speeds on the two sides of the slab. Since the Alfvén speeds themselves can be difficult to estimate, there are additional considerations we have to rely on. Once the temperature (and therefore, sound speed) information is available throughout the slab system, and one of the external Alfvén speeds (say $v_{A1}$) is known, the dependence on the second external Alfvén speed ($v_{A2}$) can easily be eliminated using the condition of total pressure balance. This way, we can estimate the internal Alfvén speed ($v_{A0}$) as a function of an external Alfvén speed ($v_{A1}$). Since Alfvén speeds are difficult to determine, measurements of multiple oscillations may be necessary to provide further information and allow us to constrain the two unknown Alfvén speeds simultaneously. A similar approach of relying on observations of multiple wave modes has already proven to be successful in, e.g., determining the density scale height in coronal loops (Andries et al. 2005), investigating the damping profiles of standing kink oscillations (Pascoe et al. 2016), and constraining parameters of flare loops (Guo et al. 2016). Special care must be taken when applying this method to the asymmetric magnetic slab system, as mode identification cannot rely solely on well-known properties of the symmetric eigenmodes (such as not displacing the center of the slab for sausage modes, or keeping the cross-sectional slab area constant for kink modes). A demonstration of the identification process and Alfvén speed inversion for single modes can be found in Allcock et al. (2019).

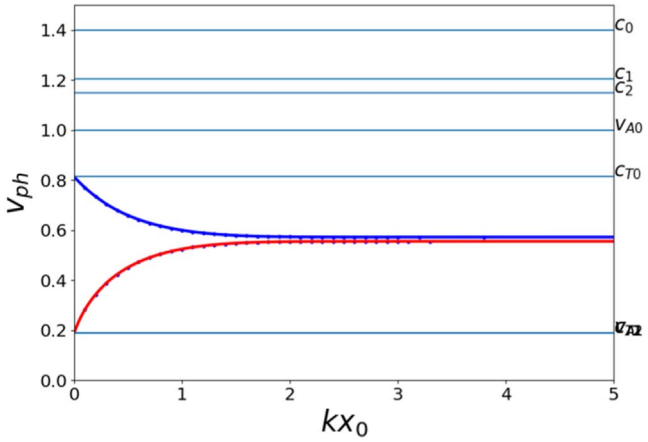


**Figure 2.** Trapped solutions in an asymmetric slab.

To complement this analysis, we also conducted a numerical investigation of the amplitude ratios of quasi-sausage modes in an asymmetric magnetic slab. First of all, we present numerical solutions of the full dispersion relation for surface modes; see Figure 2. The characteristic speeds of the three plasma regions were chosen as $v_{A0} = 1$, $c_0 = 1.4$, $v_{A1} = 0.19$, $c_1 = 1.2$, $R_1 = 1.9$, $v_{A2} = 0.18$, $c_2 = 1.09$, $R_2 = 2.28$, with the density asymmetry parameter defined in Equation (33), $\delta = 0.2$, and the magnetic asymmetry parameter defined in Equation (34), $\epsilon = 0.1$. Body mode solutions can exist between the internal tube and Alfvén speeds, but here we focus only on slow surface modes propagating with phase speeds lower than $c_{T0}$. The quasi-sausage mode is plotted in blue, while the quasi-kink mode is displayed in red. Taking the wavenumbers and the corresponding angular frequencies (or phase speeds) of these solutions, we can now calculate the amplitude ratio for the quasi-sausage waves. (Note that, in an observational example, we could take these wave parameters from the observations, and the amplitude ratios could be calculated without having to find numerical solutions to the dispersion relation.)

The amplitude ratio (Equation (16)) of slow quasi-sausage surface modes as a function of the slab width is then plotted in Figure 3, alongside its thin-slab approximation (provided in Equation (17)). The exact amplitude ratio is shown by the blue curve, while the approximation is displayed with the red points. Up to dimensionless slab width parameters of about 1, the thin-slab approximation of the amplitude ratio works relatively well, showing little deviation from the exact values. For wider slabs (or longer wavelengths), however, the differences between the estimate and the exact solution become significant. This is to be

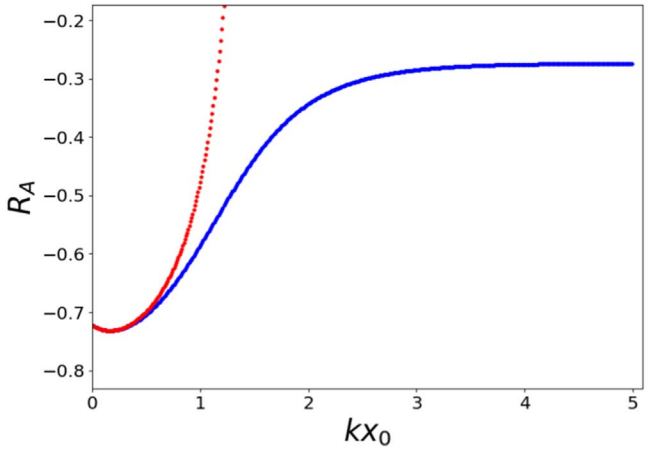


**Figure 3.** Amplitude ratios of the quasi-sausage mode as a function of $kx_0$. The exact amplitude ratio is plotted with blue, and the approximation with red.

expected, as we applied the condition $kx_0 \ll 1$ to obtain our thin-slab amplitude ratio, which may then not be valid for wide slabs.

### 2.2. Quasi-kink Modes

First, we follow the steps of the derivation process we performed for quasi-sausage modes in Section 2.1. We start by stating that, for quasi-kink modes, it is the constant $B$ that we choose arbitrarily, and we can express the rest of the coefficients as

$$A = \frac{1}{C_1 - S_1}(BC_0 - CS_0), \tag{19}$$

$$D = \frac{1}{C_2 - S_2}(BC_0 + CS_0), \tag{20}$$

$$C = \frac{\Lambda_0 S_0 + \Lambda_1 C_0}{\Lambda_0 C_0 + \Lambda_1 S_0} B = -\frac{\Lambda_0 S_0 + \Lambda_2 C_0}{\Lambda_0 C_0 + \Lambda_2 S_0} B. \tag{21}$$

The second expression for $C$ was found using the dispersion relation for the asymmetric magnetic slab system, Equation (7)). If we now substitute the first part of Equation (21) into Equation (2) describing the transverse velocity amplitudes and take the values at the two interfaces, we have

$$\hat{v}_x(-x_0) = BC_0 - CS_0 = \frac{\Lambda_0}{\Lambda_0 + \Lambda_1 \tau_0} \frac{1}{C_0} B, \text{ and} \tag{22}$$

$$\hat{v}_x(x_0) = BC_0 + CS_0 = \frac{\Lambda_0(\tau_0 + 1/\tau_0) + 2\Lambda_1}{\Lambda_0 + \Lambda_1 \tau_0} S_0 B. \tag{23}$$

Similarly, if we use the second expression from Equation (21) instead, the result for the perturbed velocity amplitudes at the slab boundaries becomes

$$\hat{v}_x(-x_0) = BC_0 - CS_0 = \frac{\Lambda_0(\tau_0 + 1/\tau_0) + 2\Lambda_2}{\Lambda_0 + \Lambda_2 \tau_0} S_0 B, \text{ and} \tag{24}$$

$$\hat{v}_x(x_0) = BC_0 + CS_0 = \frac{\Lambda_0}{\Lambda_0 + \Lambda_2 \tau_0} \frac{1}{C_0} B. \tag{25}$$

Once again, the two forms of the velocity perturbation amplitudes at the interfaces are equivalent and can be used to calculate the signed amplitude ratio, $R_A$, as

$$R_A = \frac{\Lambda_0 + \Lambda_1 \tau_0}{\Lambda_0 + \Lambda_2 \tau_0}, \tag{26}$$

or expressed with the characteristic speeds,

$$R_A = \frac{\rho_1 m_2}{\rho_2 m_1} \frac{\frac{\rho_0}{\rho_1} m_1 (k^2 v_{A0}^2 - \omega^2) + m_0 (k^2 v_{A1}^2 - \omega^2) \tau_0}{\frac{\rho_0}{\rho_2} m_2 (k^2 v_{A0}^2 - \omega^2) + m_0 (k^2 v_{A2}^2 - \omega^2) \tau_0}. \tag{27}$$

The amplitude ratio for quasi-kink modes is positive, since the displacement perturbations at the two boundaries of the slab happen in the same direction. In a symmetric slab, as expected, this ratio reduces to $R_A = 1$, showing that the symmetric kink oscillations happen exactly in phase at the boundaries of the slab.

#### 2.2.1. Quasi-kink Amplitude Ratio in the Thin-slab Approximation

In the thin-slab limit, where the width of the slab is much smaller than the wavelength of the oscillations ($kx_0 \ll 1$), the $\tanh m_0 x_0$ function can be approximated with its argument, and Equation (27) becomes

$$R_A = \frac{\rho_1 m_2}{\rho_2 m_1} \frac{\left[\frac{\rho_0}{\rho_1} m_1 (k^2 v_{A0}^2 - \omega^2) + (k^2 v_{A1}^2 - \omega^2) m_0^2 x_0\right]}{\left[\frac{\rho_0}{\rho_2} m_2 (k^2 v_{A0}^2 - \omega^2) + (k^2 v_{A2}^2 - \omega^2) m_0^2 x_0\right]}. \tag{28}$$

This equation, too, can be rearranged to give an estimate of the internal Alfvén speed in relation to measurable quantities of the asymmetric slab system and the waves that it guides:

$$v_{A0}^2 = \frac{c_0^2 \omega^2}{k^2 c_0^2 - \omega^2} + \frac{m_1 \rho_2 R_A (k^2 v_{A2}^2 - \omega^2) - m_2 \rho_1 (k^2 v_{A1}^2 - \omega^2)}{m_1 m_2 \rho_0 (1 - R_A)} x_0. \tag{29}$$

Similarly to the case of quasi-sausage modes, this expression can be used to estimate the internal Alfvén speed of oscillating solar structures as a function of only one of the external Alfvén speeds, if we express the second external Alfvén speed in terms of the other equilibrium parameters of its region using the condition of total pressure balance.

Such a formula makes it possible not only to estimate the Alfvén speed itself, but also to gauge how great of an effect the assumption of symmetry versus asymmetry in the slab model might have on the estimate. If we define Equation (29) as the asymmetric Alfvén speed (squared), $v_{AS}^2$, then we can also define the symmetric Alfvén speed, $v_S^2$, in the following manner. Let us assume that the only source of the asymmetry in the slab system is the external density difference, $\delta = (\rho_2/\rho_1) - 1$. Then, as $\delta \to 0$, it is also true that $\rho_2 \to \rho_1$, $c_2 \to c_1$, $v_{A2} \to v_{A1}$, and $m_2 \to m_1$. This allows us to simplify some terms in

Equation (29), which gives us the Alfvén speed for the symmetric case as

$$v_S^2 = \frac{c_0^2\omega^2}{k^2c_0^2 - \omega^2} + \frac{\rho_1(k^2v_{A1}^2 - \omega^2)(1 - R_A)}{\rho_0 m_1(1 - R_A)}x_0, \tag{30}$$

where $R_A \to 1$ but is not exactly one. If we now take the difference of Equations (29) and (30), we obtain

$$v_D^2 = \frac{v_{AS}^2 - v_S^2}{v_S^2} = \frac{(m_1\rho_2 R_A[k^2v_{A2}^2 - \omega^2] - m_2\rho_1 R_A[k^2v_{A1}^2 - \omega^2][R_A - 2])(k^2c_0^2 - \omega^2)x_0}{m_2(c_0^2\omega^2\rho_0 + \rho_1[k^2v_{A1}^2 - \omega^2][k^2c_0^2 - \omega^2]x_0)(1 - R_A)}, \tag{31}$$

which describes the relative error we can expect in the estimation of the Alfvén speed due to the assumption that a slab system in the solar atmosphere is symmetric, while in reality it is asymmetric.

#### 2.2.2. Amplitude Ratio in the Wide-slab Approximation

In the limit of a wide slab, the amplitude ratios of quasi-sausage and quasi-kink modes can be handled together. Now, the typical wavelength of oscillations is far shorter than the width of the slab. Therefore, $kx_0 \gg 1$, and $m_0x_0 \gg 1$. Then, both the tanh and coth functions take a value of approximately one, and the expression for the amplitude ratio becomes

$$R_A = \mp\frac{\frac{\rho_0}{\rho_1}m_1(k^2v_{A0}^2 - \omega^2) + m_0(k^2v_{A1}^2 - \omega^2)}{\frac{\rho_0}{\rho_2}m_2(k^2v_{A0}^2 - \omega^2) + m_0(k^2v_{A2}^2 - \omega^2)}, \tag{32}$$

where the negative sign corresponds to quasi-sausage modes, while the positive one describes quasi-kink waves.

### 2.3. Approximation of the Amplitude Ratios in a Weakly Asymmetric Slab

Let us now examine the dependence of the amplitude ratios on the density and magnetic field asymmetries in detail. We can define the following small quantities from the ratios of the external background parameters:

$$\delta = \frac{\rho_2}{\rho_1} - 1, \text{ and} \tag{33}$$

$$\varepsilon = \frac{B_2^2}{B_1^2} - 1. \tag{34}$$

In the following subsections, we conduct an analytical study using these parameters, and we also show a collection of numerical results on how the amplitude ratios of the eigenmodes depend on these two sources of background asymmetry.

#### 2.3.1. Quasi-sausage Modes

If we assume that both the density and the magnetic asymmetries are weak in the slab system, then both $\delta$ and $\varepsilon$ are small parameters, and we can expand the characteristic speeds on the right-hand side of the slab in terms of $\delta$ and $\varepsilon$ as

$$\begin{aligned}
v_{A2}^2 &= v_{A1}^2(1 + \varepsilon - \delta),\\
c_2^2 &= c_1^2 - \frac{\gamma}{2}v_{A1}^2\varepsilon - \delta c_1^2,\\
c_{T2}^2 &= \frac{1}{c_1^2 + v_{A1}^2}\\
&\quad\left\{c_1^2 + \left(c_1^2 - \frac{\gamma}{2}v_{A1}^2 - \frac{c_1^2\left[1 - \frac{\gamma}{2}\right]v_{A1}^2}{c_1^2 + v_{A1}^2}\right)\varepsilon - c_1^2\delta\right\}
\end{aligned} \tag{35}$$

Here, we also used the condition of total pressure balance, and we only kept first-order terms. Using the expressions thus obtained for the characteristic speeds, we can rewrite $m_2$ as

$$|m_2^2| = |m_1^2| + S(A\varepsilon + B\delta), \tag{36}$$

where

$$\begin{aligned}
A &= v_{A1}^2[m_1^2 - k^2]\left[\frac{\gamma}{2}\{k^2v_{A1}^2 - \omega^2\} - \{k^2c_1^2 - \omega^2\}\right],\\
B &= \omega^2(2\omega^2 - [\{k^2 + m_1^2\}\{c_1^2 + v_{A1}^2\}]),\\
S &= \frac{1}{2\sqrt{m_1^2}(k^2c_{T1}^2 - \omega^2)(c_1^2 + v_{A1}^2)}.
\end{aligned} \tag{37}$$

Therefore, the amplitude ratio for quasi-sausage modes in the thin-slab approximation in terms of $\varepsilon$ and $\delta$ is

$$\begin{aligned}
R_A &= -\frac{G}{L}\\
&\left(\pm 1 + \left[P - \left\{\pm\frac{N}{L}\right\}\right]\varepsilon + \left[Q - \left\{\pm\frac{M}{L}\right\}\right]\delta\right),
\end{aligned} \tag{38}$$

where

$$\begin{aligned}
G &= \rho_0 m_1 x_0[k^2v_{A0}^2 - \omega^2] + \rho_1[k^2v_{A1}^2 - \omega^2],\\
L &= \rho_0 x_0\sqrt{m_1^2}[k^2v_{A0}^2 - \omega^2] + \rho_1[k^2v_{A1}^2 - \omega^2],\\
M &= SB\rho_0 x_0[k^2v_{A0}^2 - \omega^2] - \rho_1[k^2v_{A1}^2 + \omega^2],\\
N &= SA\rho_0 x_0[k^2v_{A0}^2 - \omega^2] + \rho_1 k^2v_{A1}^2,\\
P &= \frac{SA}{m_1},\\
Q &= \frac{SB}{m_1};
\end{aligned} \tag{39}$$

To further extend the investigation of the different asymmetric effects on the amplitude ratios of the eigenmodes, we include a few illustrative numerical results as well. The top diagrams of Figure 4 show the dependence of the quasi-sausage (Figure 4(a)) and quasi-kink (Figure 4(b)) amplitude ratio on $\delta$ for a fixed value of the dimensionless slab width and the magnetic asymmetry parameter, $\varepsilon$. For the quasi-sausage modes, the exact amplitude ratio is plotted with the bright blue line, while its thin-slab approximation is shown by the dark blue dots. The bottom half shows the difference between the exact and approximate amplitude ratios ($\Delta R_A$). An

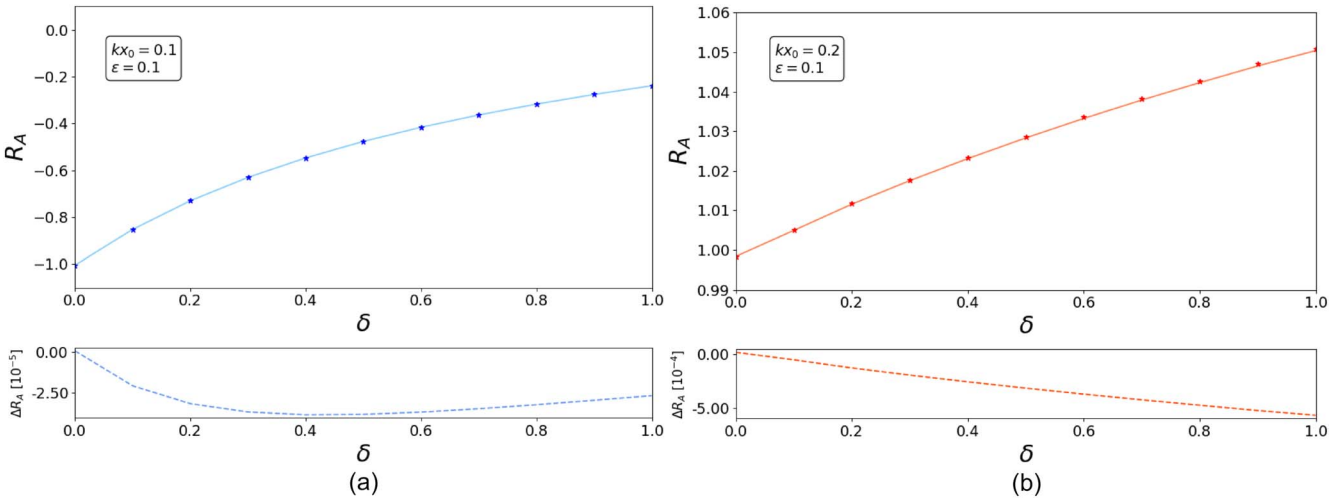


**Figure 4.** Dependence of the amplitude ratio on $\delta$, for $\epsilon = 0.1$ in the case of (a) quasi-sausage and (b) quasi-kink modes. Animated versions of these figures are available, in which the slab width changes gradually while all other parameters remain fixed.

(An animation of this figure is available.)

animated version of this figure is also available, in which it shows how the difference between the exact and approximate expressions for the amplitude ratio changes as a function of $\delta$ as the slab width is slowly increased to intermediate values. It can be concluded from these results that the difference between the exact amplitude ratio and its thin-slab approximation for quasi-sausage modes is negligibly small even for slabs of intermediate width.

From our analytical and complimentary numerical results, we can conclude that both the slab width and the density asymmetry have an important effect on the amplitude ratio. Moreover, the thin-slab approximation holds up very well for the changing values of delta, even as far up as $\delta = 3$, which would mean a rather high density asymmetry ($\rho_2$ is four times as large as $\rho_1$). However, all of this is only true for slab width values up to about $kx_0 = 0.7$, which is where the amplitude ratio obtained from the thin-slab approximation visibly starts to differ from the actual value. We also have to keep in mind that our numerical examples only encompass a chosen set of characteristic speed parameters, and different plasma-$\beta$ values in the three regions of the model might lead to amplitude ratios that show larger and/or smaller deviations from their thin-slab approximation.

#### 2.3.2. Quasi-kink Modes

Through a similar process, we now express the amplitude ratio for quasi-kink modes in terms of the density and magnetic asymmetries (to first order) in the following form:

$$R_A = \frac{T}{U}\left(\pm + \left[P - \pm\frac{V}{U}\right]\varepsilon + \left[Q - \pm\frac{W}{U}\right]\delta\right), \tag{40}$$

where

$$\begin{aligned} T &= \rho_0 m_1[k^2 v_{A0}^2 - \omega^2] + \rho_1[k^2 v_{A1}^2 - \omega^2] m_0^2 x_0, \\ U &= \rho_0\sqrt{m_1^2}\,[k^2 v_{A0}^2 - \omega^2] + \rho_1 m_0^2 x_0[k^2 v_{A1}^2 - \omega^2], \\ V &= SA\rho_0[k^2 v_{A0}^2 - \omega^2] + \rho_1 m_0^2 x_0 k^2 v_{A1}^2, \\ W &= SB\rho_0[k^2 v_{A0}^2 - \omega^2] + \rho_1 m_0^2 x_0[k^2 v_{A1}^2 + \omega^2], \end{aligned} \tag{41}$$

Similarly to Figure 4(a), panel (b) of that figure displays the dependence of the amplitude ratio of the quasi-kink modes on the density asymmetry $\delta$, for the same characteristic speeds as before, and $kx_0 = 0.2$. An animated version of this figure is also available, which illustrates how the exact and approximate amplitude ratios change as the dimensionless slab width slowly increases. For the chosen values of background parameters, at least, from small up to intermediate slab widths expressed in their dimensionless measure, the difference between the dependence of the amplitude ratio on the density asymmetry calculated from the exact general formula and the thin-slab approximation is still relatively small. Along with the difference, the density dependence itself also displays a much stronger effect on the magnitude of the amplitude ratio for higher values of the slab width.

## 3. Minimum Perturbation Shift

The second spatial magneto-seismology technique we describe here is one that describes the shift in the position of minimum wave power away from the center of an asymmetric slab. The position of the minimally perturbed surface for a symmetric sausage or kink mode lies at exactly the central axis of the slab ($x = 0$). We define the minimum perturbation shift, $\Delta_{\min}$, as the offset of the minimum wave power from the center of the slab, as illustrated for a quasi-kink mode in Figure 5. The method of the minimum perturbation shift is exclusive to surface modes, which, as was shown in Zsámberger & Erdélyi (2020), are significantly more sensitive to the external plasma parameters than body modes. Body modes show a shift in the position of their nodes and anti-nodes under the effect of external asymmetries; however, this is expected to be a much smaller and therefore less easily observable quantity (see also Allcock & Erdélyi 2018).

### 3.1. Quasi-sausage Modes

For a symmetric slab system, the sausage modes leave the surface in the center of the slab unperturbed. When density and/or magnetic asymmetry is introduced into the environment, the

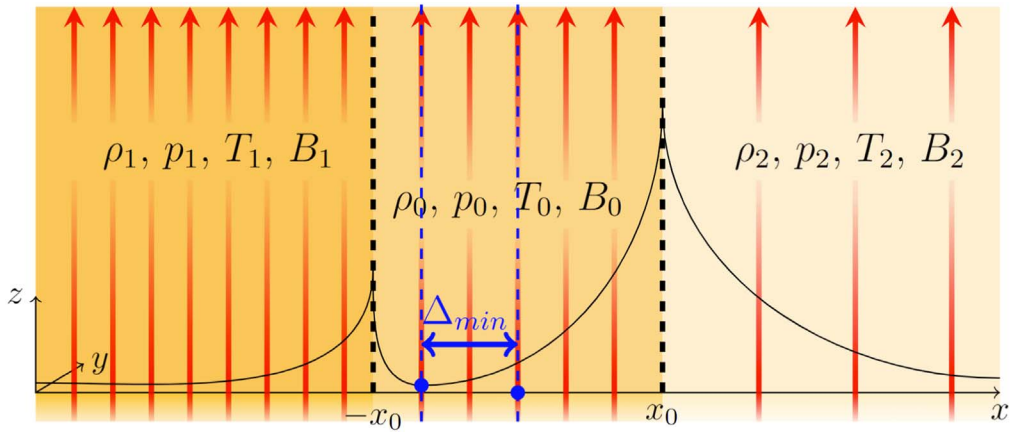


**Figure 5.** The principle of the minimum perturbation shift method. Figure courtesy of Allcock & Erdélyi (2018).

position of this surface is shifted away from the middle to a new $x$-coordinate that can be found simply by setting the transverse velocity perturbation amplitude,

$$\hat{v}_x(x) = B\cosh m_0 x + C\sinh m_0 x = 0, \tag{42}$$

from which $x$ can be expressed as

$$x = \frac{1}{m_0}\tanh^{-1}\left\{-\frac{B}{C}\right\}, \tag{43}$$

where $|x| \leqslant x_0$. Using the equations describing the continuity of velocity and total pressure perturbations at the boundaries of the slab, the coefficient $B$ can be expressed in two different forms described in Equation (6). Substituting this into Equation (43), the $x$-coordinate of the minimally perturbed surface, $\Delta_{\rm min}$, becomes

$$\begin{aligned}\Delta_{\rm min} &= \frac{1}{m_0}\tanh^{-1}\left\{-\frac{\Lambda_0 C_0 + \Lambda_1 S_0}{\Lambda_0 S_0 + \Lambda_1 C_0}\right\} \\ &= \frac{1}{m_0}\tanh^{-1} \\ &\left\{-\frac{\frac{\rho_0}{\rho_1}m_1[k^2 v_{A0}^2 - \omega^2] + m_0[k^2 v_{A1}^2 - \omega^2]\tau_0}{\frac{\rho_0}{\rho_1}m_1[k^2 v_{A0}^2 - \omega^2]\tau_0 + m_0[k^2 v_{A1}^2 - \omega^2]}\right\}.\end{aligned} \tag{44}$$

In the thin-slab approximation, as we have stated before, $kx_0 \ll 1$, and so $m_0 x_0 \ll 1$. Then, it is also true that the minimum perturbation shift is $\Delta_{\rm min} < x_0$ and therefore $m_0\Delta_{\rm min} \ll 1$. In this case, the hyperbolic tangent can be approximated by its argument, and Equation (44) can be rearranged to provide another estimate for the internal Alfvén speed as a function of the slab width, the minimum perturbation shift, and the external parameters on one side of the slab, as well as the internal density and sound speed:

$$\begin{aligned}v_{A0}^2 = &\frac{(k^2 c_0^2 - \omega^2)x_0\Delta_{\rm min} + c_0^2}{(k^2 c_0^2 - \omega^2)(k^2 x_0\Delta_{\rm min} + 1)}\omega^2 \\ &-\frac{(x_0 + \Delta_{\rm min})(k^2 v_{A1}^2 - \omega^2)}{\rho_0/\rho_1 m_1(k^2 x_0\Delta_{\rm min} + 1)}.\end{aligned} \tag{45}$$

The minimum perturbation shift is ill-defined in the wide-slab limit, when $kx_0 \gg 1$, where the two interfaces oscillate basically independently of one another at their own eigen-frequency (see also Allcock & Erdélyi 2018).

### 3.2. Quasi-kink Modes

Symmetric kink modes are characterized by causing zero perturbation along the central surface of the slab, too. Asymmetric quasi-kink modes, on the other hand, only possess a surface of minimum perturbation (where the transverse velocity perturbation is smallest, but not necessarily zero), which is, again, shifted from the center of the slab. The $x$-coordinate of this least-perturbed surface can be determined by finding where the derivative of the transverse velocity perturbation is zero:

$$\frac{d\hat{v}_x(x)}{dx} = m_0(B\sinh m_0 x + C\cosh m_0 x) = 0. \tag{46}$$

From this, the required $x$-coordinate can be expressed as

$$x = \frac{1}{m_0}\tanh^{-1} - \frac{C}{B} = \frac{1}{m_0}\coth^{-1} - \frac{B}{C}. \tag{47}$$

Now, substituting the forms of the $C$ coefficients from Equation (21) into this expression gives us the $x$-coordinate of the minimally perturbed surface, $\Delta_{\rm min}$, as

$$\begin{aligned}\Delta_{\rm min} &= \frac{1}{m_0}\coth^{-1}\left\{-\frac{\Lambda_0 C_0 + \Lambda_1 S_0}{\Lambda_0 S_0 + \Lambda_1 C_0}\right\} \\ &= \frac{1}{m_0}\coth^{-1} \\ &\left\{-\frac{\frac{\rho_0}{\rho_1}m_1[k^2 v_{A0}^2 - \omega^2] + m_0[k^2 v_{A1}^2 - \omega^2]\tau_0}{\frac{\rho_0}{\rho_1}m_1[k^2 v_{A0}^2 - \omega^2]\tau_0 + m_0[k^2 v_{A1}^2 - \omega^2]}\right\}.\end{aligned} \tag{48}$$

Applying the thin-slab approximation allows us to provide an estimate for the internal Alfvén speed in the case of the quasi-kink modes, too, following a similar reasoning as we used to obtain Equation (45) for quasi-sausage modes. Here, the internal Alfvén speed can be approximated as

$$v_{A0}^2 = \frac{-B \pm \sqrt{B^2 - 4AC}}{2A}, \tag{49}$$

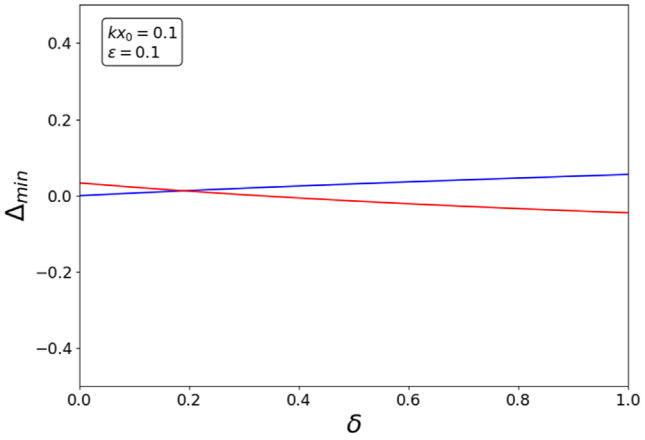


**Figure 6.** Dependence of the minimum perturbation shift of the quasi-sausage (blue) and quasi-kink mode (red) on $\delta$, for $\epsilon = 0.1$ and $kx_0 = 0.1$. An animated version of this figure is also available, in which the slab width slowly increases frame by frame.

(An animation of this figure is available.)

where

$$A = (k^2c_0^2 - \omega^2)\frac{\rho_0}{\rho_1}k^2m_1\Delta_{\min},$$
$$B = (k^2c_0^2 - \omega^2)\left([k^2v_{A1}^2 - \omega^2]\left[\frac{\rho_0}{\rho_1}m_1x_0 + 1 + k^2\Delta_{\min}x_0\right] - \frac{\rho_0}{\rho_1}\omega^2m_1\Delta_{\min}\right),$$
$$C = (k^2v_{A1}^2 - \omega^2)\left(\left[\frac{\rho_0}{\rho_1}m_1x_0 + 1\right]c_0^2 + (k^2c_0^2 - \omega^2)\Delta_{\min}x_0\omega^2\right). \quad (50)$$

The dependence of the minimum perturbation shift of the eigenmodes of an asymmetric magnetic slab system on the density asymmetry, $\delta$, for a given fixed value of the magnetic asymmetry parameter, $\varepsilon$, is displayed in Figure 6, for the same characteristic speeds as all other figures in this paper. An animated version of this figure is also available as supplementary material, showing how the $\delta$-dependence of both modes becomes more prominent for higher values of the dimensionless slab width. Of course, this is only an illustrative example of the perturbation shift method, and the solutions might behave differently for an alternative characteristic speed ordering, which was beyond the scope of the current investigation.

### 3.3. The Incompressible Limit

One last approximation that is interesting to investigate is that of the system being filled with incompressible magnetized plasma. In this case, the sound speeds are unbounded, so that $m_j = k$, for $j$=0, 1, 2. Then, the minimum perturbation shift for quasi-sausage (top) and quasi-kink modes (bottom) can be expressed as

$$\Delta_{\min} = \frac{1}{k}\begin{pmatrix}\tanh^{-1}\\ \coth^{-1}\end{pmatrix}\left\{-\frac{\frac{\rho_0}{\rho_1}[v_{A0}^2 - \omega^2] + [k^2v_{A1}^2 - \omega^2]\tanh[kx_0]}{\frac{\rho_0}{\rho_1}[v_{A0}^2 - \omega^2]\tanh[kx_0] + [k^2v_{A1}^2 - \omega^2]}\right\}. \quad (51)$$

This can be rearranged to provide a relatively simple estimate for the internal Alfvén speed in terms of an external Alfvén speed and density ratio, as well as measurable wave and geometric parameters of the slab system:

$$v_{A0}^2 = \frac{\omega^2}{k^2}\left(1 - \frac{\rho_1[k^2v_{A1}^2 - \omega^2]}{\rho_0\omega^2}\begin{pmatrix}\tanh\\ \coth\end{pmatrix}\{k[x_0 + \Delta_{\min}]\}\right). \quad (52)$$

While this provides a simple approximation of the internal Alfvén speed in an asymmetric slab system, here we must remind the reader that, e.g., the upper solar atmosphere in general is not an incompressible plasma environment. However, kink perturbations in the long wavelength can be considered incompressible in linear order. Therefore, even this simple expression can provide a first insight into the parameters of a magnetized plasma slab going through kink oscillations. Then, as a next step, the Alfvén speed estimate obtained with the incompressible approximation can be compared to estimates resulting from other methods to validate the employed method or explore its limitations.

## 4. Discussion

In this paper, we provided results we obtained for developing further solar magneto-seismology tools for asymmetric slab systems, which rely on the change in character occurring in the eigenmodes supported by a waveguide that is under the effect of its asymmetric environment. Both of the methods described here belong under the wider umbrella of spatial magneto-seismology, which, as opposed to temporal seismology methods, has had a shorter history and a recent "golden age" thanks to the rapidly increasing observational capabilities of solar telescopes.

We have provided a derivation for two SMS techniques introduced by Allcock & Erdélyi (2018) for an asymmetric magnetic slab placed in a nonmagnetic environment, and we have generalized them to the case of a magnetic slab enclosed in an asymmetric magnetic environment. Section 2 describes the amplitude ratio method, which relies on the fact that the ratio of oscillation amplitudes at the two boundaries of the slab deviates from unity for general asymmetric eigenmodes. We provided an exact formula for the amplitude ratios of both quasi-sausage and quasi-kink modes, and then we proceeded to include some analytical approximations of these in order to make inversion possible and derive estimates for the Alfvén speed within the slab in terms of the rest of the equilibrium background parameters, as well as the frequencies and wavenumbers of oscillations.

Next, in Section 3, we generalized the minimum perturbation shift method to asymmetric slab systems including external magnetic asymmetry next to the density asymmetry. Deriving magnetic field information—directly, e.g., from Stokes parameters, or indirectly via a proxy, e.g., from the Alfvén speed—is an important quest in solar physics. The application of the minimum shift theorem provides a new, additional method to further our efforts in such quests. This tool allows us to express new estimates for the Alfvén speed within the slab model in the analytical limit of a thin or an incompressible slab. All of the Alfvén speed estimates the application of this method provides show a dependence on a *measurable* asymmetric spatial parameter of waves (either the amplitude ratio or the minimum perturbation shift), the wavenumber and frequency of the eigenmodes, the geometric extent of the slab, and at least one external density and Alfvén speed.

It is often the case that multiple plasma or magnetic parameters of a solar atmospheric structure are unknown. However, if we use wave parameters measured in a solar atmospheric structure, where the slab model is a feasible approximation, we only have to provide an estimate for some of the unknown external parameters in order to use the formulae derived here. If, however, one wanted to apply them to all possible eigenmodes supported by a given asymmetric slab system, an implicit dependence on the remaining external parameters would also have to be taken into account when solving the dispersion relation to obtain the angular frequencies and wavenumbers of trapped oscillations. Last but not least, it needs to be remarked that asymmetry does not seem to have a dominant effect on the wave parameters of oscillating waveguides over all other determining factors, such as structuring, dynamics, geometry, or nonideal effects. For example, when investigating the frequencies of standing waves in asymmetric slabs, Oxley et al. (2020a) found that the width of the slab had a stronger influence on the frequencies of harmonics than the external asymmetry. However, one cannot know the relative magnitudes of the influences of all the effects listed above in advance, therefore all these studies need to be carried out. Additionally, measuring asymmetry may allow us to confirm or refute estimates of solar atmospheric parameters made in alternative ways, and this is a point that one may wish to bear in mind when carrying out SMS studies.

R.E. is grateful to the Science and Technology Facilities Council (STFC, grant No. ST/M000826/1) for the support received. N.Z. is grateful for the support of the University of Debrecen and the University of Sheffield. All numerical results are derived using Python, an open-source and community-developed programming language. The authors thank M. Barbulescu for the basis of the root-finding algorithm used during the numerical investigation, available at https://github.com/BarbulescuMihai/PyTES.

## ORCID iDs

Noémi Kinga Zsámberger https://orcid.org/0000-0002-2822-129X
Róbert Erdélyi https://orcid.org/0000-0003-3439-4127

## References

Allcock, M., & Erdélyi, R. 2017, SoPh, 292, 35
Allcock, M., & Erdélyi, R. 2018, ApJ, 855, 90
Allcock, M., Shukhobodskaia, D., Zsámberger, N. K., & Erdélyi, R. 2019, FrASS, 6, 48
Andries, J., Arregui, I., & Goossens, M. 2005, ApJL, 624, L57
Arregui, I. 2015, RSPTA, 373, 20140261
Arregui, I., & Goossens, M. 2019, A&A, 622, A44
Arregui, I., Oliver, R., & Ballester, J. L. 2012, LRSP, 9, 2
Aschwanden, M. 2005, Physics of the Solar Corona (Berlin: Springer)
Aschwanden, M. J., Fletcher, L., Schrijver, C. J., & Alexander, D. 1999, ApJ, 520, 880
Banerjee, D., Erdélyi, R., Oliver, R., & O'Shea, E. 2007, SoPh, 246, 3
De Moortel, I., & Nakariakov, V. M. 2012, RSPTA, 370, 3193
Edwin, P. M., & Roberts, B. 1982, SoPh, 76, 239
Erdélyi, R. 2006a, RSPTA, 364, 351
Erdélyi, R. 2006b, ESA Special Publication, Vol. 624, Proc. of SOHO 18/GONG 2006/HELAS I, Beyond the spherical Sun (Noordwijk: ESA), 15.1
Erdélyi, R., Hague, A., & Nelson, C. 2014, SoPh, 289, 167
Erdélyi, R., & Verth, G. 2007, A&A, 462, 743
Goossens, M., Andries, J., & Aschwanden, M. J. 2002, A&A, 394, L39
Goossens, M., Terradas, J., Andries, J., Arregui, I., & Ballester, J. L. 2009, A&A, 503, 213
Guo, M.-Z., Chen, S.-X., Li, B., Xia, L.-D., & Yu, H. 2016, SoPh, 291, 877
Hollweg, J. V., Yang, G., Cadez, V. M., & Gakovic, B. 1990, ApJ, 349, 335
Mathioudakis, M., Jess, D. B., & Erdélyi, R. 2013, SSRv, 175, 1
Nakariakov, V. M., Ofman, L., Deluca, E. E., Roberts, B., & Davila, J. M. 1999, Sci, 285, 862
Nakariakov, V. M., & Verwichte, E. 2005, LRSP, 2, 3
Oxley, W., Zsámberger, N. K., & Erdélyi, R. 2020a, ApJ, 890, 109
Oxley, W., Zsámberger, N. K., & Erdélyi, R. 2020b, ApJ, 898, 19
Pascoe, D. J., Goddard, C. R., Nisticò, G., Anfinogentov, S., & Nakariakov, V. M. 2016, A&A, 585, L6
Roberts, B. 1981a, SoPh, 69, 27
Roberts, B. 1981b, SoPh, 69, 39
Roberts, B., Edwin, P. M., & Benz, A. O. 1984, ApJ, 279, 857
Rosenberg, H. 1970, A&A, 9, 159
Ruderman, M. S., & Erdélyi, R. 2009, SSRv, 149, 199
Ruderman, M. S., & Roberts, B. 2002, ApJ, 577, 475
Uchida, Y. 1970, PASJ, 22, 341
Verth, G., Van Doorsselaere, T., Erdélyi, R., & Goossens, M. 2007, A&A, 475, 341
Wang, T. 2011, SSRv, 158, 397
Zaqarashvili, T. V., & Erdélyi, R. 2009, SSRv, 149, 355
Zsámberger, N. K., Allcock, M., & Erdélyi, R. 2018, ApJ, 853, 136
Zsámberger, N. K., & Erdélyi, R. 2020, ApJ, 894, 123
Zsámberger, N. K., & Erdélyi, R. 2021, ApJ, 906, 122